methane

MDPI

Article

Expanded Reactor Engineering Calculations for the Oxidative Coupling of Methane

Andrin Molla, Sonya Rivera, Phillip Pera, Michael Landaverde and Robert Barat *

Otto H. York Department of Chemical and Materials Engineering, New Jersey Institute of Technology, Newark, NJ 07102, USA; am492@njit.edu (A.M.); sr367@njit.edu (S.R.); pp523@njit.edu (P.P.); msl27@njit.edu (M.L.)

* Correspondence: barat@njit.edu

Abstract: The catalytic activation of CH_4 by limited amounts of O_2 produces a mixture of synthesis gas (CO, H_2) and light hydrocarbons (C_2H_x), the relative amounts of each depending on catalyst type and process conditions. Using an elementary reaction mechanism for the oxidative coupling of methane (OCM) on a La_2O_3/CeO_2 catalyst derived from the literature, this study replaces the activating O_2 with moist H_2O_2 vapor to reduce synthesis gas production while improving C_2H_x yields and selectivities. As the H_2O_2 content of the activating oxidant rises, more of the CH_4 conversion occurs in the gas phase instead of with the catalytic surface. In a packed bed reactor (PBR), the use of H_2O_2 allows the PBR "light-off" to occur using a lower feed temperature. In exchange for a small decline in CH_4 conversion, C_2H_x selectivity increases while synthesis gas production drops. In a continuous stirred tank reactor (CSTR), H_2O_2 improves C_2H_x over synthesis gas across a wider range of feed temperatures than is possible with the PBR. This suggests the CSTR will likely reduce OCM preheating requirements.

Keywords: catalyst; coupling; methane; peroxide; oxidative

check for updates

Citation: Molla, A.; Rivera, S.; Pera, P.; Landaverde, M.; Barat, R. Expanded Reactor Engineering Calculations for the Oxidative Coupling of Methane. *Methane* **2022**, *1*, 58–69. https://doi.org/10.3390/methane1010005

Academic Editor: Mateusz Wnukowski

Received: 12 January 2022
Accepted: 2 February 2022
Published: 11 February 2022

Publisher's Note: MDPI stays neutral with regard to jurisdictional claims in published maps and institutional affiliations.

Copyright: © 2022 by the authors. Licensee MDPI, Basel, Switzerland. This article is an open access article distributed under the terms and conditions of the Creative Commons Attribution (CC BY) license (https://creativecommons.org/licenses/by/4.0/).

1. Introduction

The expanded use of hydraulic fracturing has resulted in the venting and flaring of large volumes of hydrocarbons, especially natural gas. A lack of local pipeline capacity results in more flaring [1] and fugitive emissions. Public sentiment is prompting government environmental regulators to force the reduction or outright banning of hydrocarbon flaring and fugitive emissions [2] to reduce climate change by global warming. Petroleum and natural gas companies are now actively promoting their efforts to reduce their methane footprints [3]. However, the engineering challenge of CH_4 conversion is considerable. Catalytic methods offer several conversion approaches.

Catalytic activation of CH_4 is generally classified as indirect or direct. Indirect activation produces synthesis gas (primarily CO and H_2) using an oxygen source by reforming (H_2O—steam; CO_2—dry) or partial oxidation (O_2). Synthesis gas can be catalytically converted to useful products such as alcohol (usually CH_3OH) or higher hydrocarbons (by Fischer–Tropsch process).

Direct activation of CH_4 uses no oxygen source. It directly breaks the very strong CH_3–H bond (4.39×10^5 J/mol). For example, methane dehydroaromatization (MDA) uses a Mo/HZSM-5 zeolite [4] catalyst to form C_2H_4 and aromatics at 950–1030 K. Unfortunately, MDA is thermodynamically limited. In addition, catalyst activity drops quickly due to coke deposition.

An intermediate direct approach is the oxidative coupling of methane (OCM) that uses a very small amount of O_2 to activate the CH_4 while limiting the coke formation. The OCM catalysts are transition metal oxides on an oxide support, e.g., La_2O_3/CaO [5] and La_2O_3/CeO_2 [6]. Feed CH_4/O_2 molar ratios of 7–11 with temperatures ~840–1220 K

have been studied. The products include $C_{2+}H_x$ and synthesis gas, with the distribution depending on the catalyst and temperature. More feed O_2 favors CH_4 conversion, but lowers $C_{2+}H_x$ selectivity in favor of CO_x.

Gambo et al. [7] reviewed recent advances in OCM, including the use of catalyst nanowires, and identified avenues for further research. Using proprietary nanowire catalysts, Siluria Technologies demonstrated OCM in a continuous flow large demonstration plant [8,9]. The primary goal is the production of C_2H_4 for subsequent conversion to gasoline and chemicals. Siluria envisions a flexible two-stage OCM reactor in which the first stage is a packed bed reactor (PBR) feeding CH_4, O_2, and possibly C_2H_6. The second stage feeds more C_2H_6 in an endothermic pyrolysis plug flow reactor that uses the first stage exothermicity.

Considering the potential and the constraints of OCM, the reactor type becomes important. Conventional packed beds are not economically viable for OCM [10]. Other configurations such as membrane reactors and fluidized beds should be considered. A recent study [11] compared the packed bed reactor (PBR) and continuous stirred tank reactor (CSTR) for OCM based on calculations with a detailed reaction mechanism [6]. Higher feed temperatures were required to achieve a "light off" of the PBR, while the CSTR required considerably lower feed temperatures to reach nearly comparable conversions. The CSTR—a fluidized bed in likely practice—favored synthesis gas production over $C_{2+}H_x$ as compared to the PBR.

In a difficult experimental study, Liu et al. [12] considered the rapid PBR "light off". Using careful temperature control and real-time product measurement in a micro-reactor during OCM over La_2O_3 nanorod catalysts with a feed $CH_4/O_2 = 3$, Liu et al. observed that CO_2 is the dominant product at the lower temperatures (<853 K) when relative O_2 concentrations are high. The system transitions through a window (~873 K) to higher temperatures (>913 K) that favor $C_{2+}H_x$ at the lower O_2 levels. In effect, a competition between CO_x and $C_{2+}H_x$ formation occurs in this window. This suggests that reactor configuration and temperature will be critical for OCM reactor design. These observations also show that, in OCM, the production of byproduct syngas is unavoidable if $C_{2+}H_x$ is the goal.

In typical OCM, some of the limited O_2 dissociates on the catalyst surface [13]. An adsorbed $\bullet O_s$ then abstracts an H• from CH_4 to form the key $\bullet CH_3$ gas phase radical. Oxygen atoms on the metal oxide lattice surface might directly abstract the H• from CH_4. In this case, the gas phase O_2 replenishes the resulting surface vacancy, leaving behind an adsorbed $\bullet O_s$ [7]. In either case, the $\bullet CH_3$ radicals can combine to form C_2H_6. Further reactions form the desired $C_{2+}H_x$ products, and the undesired CO_x and coke. An alternate CH_3-H bond activator would reduce CO_x while possibly enhancing $C_{2+}H_x$ formation. Unfortunately, the desired $C_{2+}H_x$ products are more susceptible to oxidation than the reactant CH_4. This can occur via gas phase O_2 or surface oxygen species [7,13].

An alternate or supplementary oxidant that might be less aggressive toward $C_{2+}H_x$ by reducing surface oxygen species while still activating the CH_4 is the •OH gas phase radical. Gas phase hydroxyl radicals can be formed from the gas phase decomposition of co-fed H_2O_2 vapor: $H_2O_2 + M = 2 \bullet OH + M$. Section 3 below summarizes experimental literature on the use of H_2O_2 for OCM that motivates this paper.

This paper is also a sequel to the Rivera et al. [11] study on OCM. It uses the same elementary reaction mechanism as that developed by Karakaya et al. [6]. The paper considers vapor phase H_2O_2 as a supplemental or alternative activating oxidizer to reduce syngas production in favor of $C_{2+}H_x$. Both CSTR and PBR are considered.

2. Kinetic Mechanism and Computational Tool

The detailed reaction mechanism used in this study was developed by Karakaya et al. [6]. It is composed of series and parallel elementary reactions [13] in both the gas and surface phases. The gas phase portion is taken from Chen et al. [14]. The surface portion is inspired by the work of Alexiadis et al. [15].

In the current study, the OCM mechanism was employed in reactor simulations by Detchem® [16]. This program achieves material and energy balances using the mechanism, based on required reactor input data and parameters. In this study, separate adiabatic PBR (modeled as plug flow) and CSTR (modeled as perfectly mixed) runs were conducted with the Detchem® PBED and CSTR applications, respectively. See [11] for a listing of the governing balance equations used in each reactor simulation.

Comparative results were prepared in terms of conversions X_{CH4}, selectivities S_j of useful products (C_2H_x, CO, H_2) or byproducts (H_2O, CO_2), and yields Y_j:

$$X_{CH_4} \equiv \frac{F_{CH_4,in} - F_{CH_4}}{F_{CH_4,in}} \; X_{O_2} \equiv \frac{FO_{2,in} - F_{O_2}}{F_{O_2,in}} \; S_j \equiv \frac{n_j F_j}{F_{CH_4,in} - F_{CH_4}} \; Y_j \equiv \frac{n_j F_j}{F_{CH_4,in}} \quad (1)$$

where F_j = molar flow rates, $F_{j,in}$ = molar rate at the reactor inlet, and n_j is the number of CH_4 moles needed to make one mole of product (byproduct). For example, for C_2H_4, $n_j = 2$; for H_2, $n_j = 0.5$.

In the prior study [11] of OCM with O_2 (no H_2O_2) as the activator, twenty cases were considered in separate CSTR and PBR calculations. The process parameters considered are summarized in Table 1. The parametric study included the molar feed CH_4/O_2 ratio ("low" = 7, "high" = 11; LR and HR, respectively), molar feed rate ("low" = 8.984×10^{-5}, "high" = 1.412×10^{-4} mole/s; called LF and HF, respectively), and feed temperature (843–1243). At each of the five feed temperatures, four cases were considered: LR_LF, LR_HF, HR_LF, and HR_HF. These conditions were inspired by published laboratory data [6]. Each reactor simulation assumed the same catalytic site density and total catalytic surface area, resulting in the same 2.42×10^{-6} total moles of sites. A processing rate can be defined as the ratio of total molar feed rate to the total number of catalyst sites. The processing rate range is 37.1–58.3 s^{-1}. These parameters motivate the present study. Larger reactors can be scaled from these conditions.

Table 1. Process parameters of this study, inspired by Karakaya et al. [6].

Low Feed Ratio "LR" CH_4/O_2 or CH_4/H_2O_2 = 7			High Feed Ratio "HR" CH_4/O_2 or CH_4/H_2O_2 = 11	
Low Feed Processing Rate "LF" 37.1/s			High Feed Processing Rate "HF" 58.3/s	
Feed Temperatures T_{in} (K)				
843	943	1043	1143	1243

3. Alternate Activator H_2O_2

Garibyan et al. [17] studied OCM over Pb/aerosil, ZnO, and 10% Na_2O/ZnO catalysts. Pulses of H_2O_2 vapor into the CH_4/O_2 feed increased the C_2H_x yield while stabilizing catalytic activity during OCM at 1 atmosphere and 1023 K. With a 1% Au/5% La_2O_3/CaO catalyst, at 973–1073 K, Eskendirov et al. [18,19] observed that H_2O_2 increased CH_4 conversion, while enhancing C_{2+} hydrocarbon yields even up to benzene. They speculated that H_2O_2 decomposition resulted in more •OH radicals for gas phase activation of the CH_4. They even observed OCM in the presence of H_2O_2 vapor without catalyst at temperatures as low as 673 K, with considerable selectivity for C_2H_x. These studies motivate this paper.

Considering the importance of making any OCM process as "green" as possible, a potentially sustainable source of H_2O_2 uses a photo-activated TiO_2-Au-Si catalyst while feeding O_2 and liquid H_2O [20]. Spiegelman and Alvarez [21] developed a simple yet clever technology to produce a continuous vapor stream of H_2O_2 from a liquid solution of H_2O_2 in water. Subsequent drying of the vapor stream to raise the H_2O_2 concentration runs the risk of energetic decomposition, thus posing a safety risk. In a study of the decomposition of H_2O_2 vapor on various surfaces, Satterfield and Stein [22] generated H_2O_2 vapor concentrations of up to 0.23 atm in a 1 atm system. Therefore, in the remainder

of these calculations, we used a conservative molar H_2O/H_2O_2 = 4 linkage in all cases where H_2O_2 was used.

The OCM process requires considerable preheating, so the H_2O_2 decomposition risk also calls into question the feed temperature for the H_2O/H_2O_2 vapor stream. Consider the decomposition: H_2O_2 + M → 2 •OH + M with a rate constant borrowed from the Chen et al. [14] reaction set for the CH_4 gas phase chemistry used in the OCM mechanism [6]. Assume a feed CH_4/H_2O_2 ratio of 11 (the HR case), with the coflowing H_2O vapor, and no O_2. A simple kinetic calculation shows that, at 1243 K, the H_2O_2 will be 100% decomposed in 10 microseconds. At 673 K, the time is a more realistic 5 s. This simple calculation suggests that preheating a combined CH_4, O_2, H_2O_2, and H_2O feed stream would be problematic, especially for a PBR. It also suggests keeping the CH_4/O_2 and H_2O/H_2O_2 vapor streams separate, with the CH_4/O_2 stream taking most or all the preheat. Separate feed streams are more easily handled with the CSTR.

Finally, the replacement of O_2 by H_2O_2 maintains the feed CH_4-to-O molar ratio, though it somewhat increases the overall H content of the feed. Consider the following overall reactions below. Though simplistic, Equations (1) and (2) show that replacing O_2 with H_2O_2 should increase the production of C_2H_4 and H_2O, while reducing CO and H_2. In addition, adiabatic reactor temperatures should be lower.

$$CH_4 + 0.5\,O_2 = \frac{1}{3}C_2H_4 + \frac{2}{3}H_2O + \frac{1}{3}CO + \frac{2}{3}H_2 \quad \Delta H_r^o = -105.7\ \mathrm{kJ/mole} \tag{2}$$

$$CH_4 + 0.5\,H_2O_2 = 0.5\,C_2H_4 + H_2O + 0.5\,H_2 \quad \Delta H_r^o = -72.7\ \mathrm{kJ/mole} \tag{3}$$

3.1. Incremental H_2O_2 Replacing O_2 to PBR at Fixed Feed Temperature

Rivera et al. [11] showed that, for the parametric range considered (Table 1), the highest CH_4 conversions for the PBR were nearly 40% for the LR cases, with little impact of flow rate, for a 1243 K feed temperature. The LR_LF case showed the highest sum_C_2H_x (sum of C_2H_6, C_2H_4, and C_2H_2) selectivities and yields. First, for the same 1243 K feed temperature, H_2O_2 was incrementally substituted for O_2. It was assumed that H_2O_2 vapor will be available at 20 mole percent with the balance of H_2O vapor. The starting point was the LR_LF (feed CH_4/O_2 = 7, feed processing rate 37.1/s) case [11] in the PBR. The PBR bed length was that used in the experiments described elsewhere [6]. This high feed temperature did ignore the H_2O_2 stability issue. The insights gained, however, will help identify the utility of H_2O_2 as a potential CH_4 activator.

Figure 1 shows that the final PBR bed temperature drops with increasing H_2O_2 content. This was attributed to the reduced overall reaction exothermicity suggested by Equations (1) and (2). However, the bed temperature peaked much earlier when H_2O_2 was used in the feed oxidant. A closer examination of the post-entrance region is revealed in Figure 2 below. The H_2O_2-containing cases showed a near-immediate rise from the 1243 K feed temperature. The very early single peak for the R = 1 (no feed O_2) case roughly corresponded to the exhaustion of the H_2O_2, which was consistent with the extremely rapid H_2O_2 decomposition described earlier at this temperature. The presence of the feed O_2 caused a second local temperature peak further downstream. These peaks (R = 0.33, 0.67 cases) and the much later single peak (R = 0) corresponded approximately to where the O_2 ran out, with no further adsorbed •O_s.

The R = 1 case (no feed O_2) showed almost no adsorbed species, suggesting that all the CH_4 conversion effectively occurred in the gas phase (i.e., non-catalytic). On the contrary, for the R = 0.33 and 0.67 cases, while H_2O_2 was still present, there was a complex parallel/series scheme ongoing with both catalytic and gas-phase reactions occurring. These observations were consistent with the claim that the CH_4 conversion is accelerated by •OH gas phase radicals produced from the H_2O_2 dissociation [18,19].

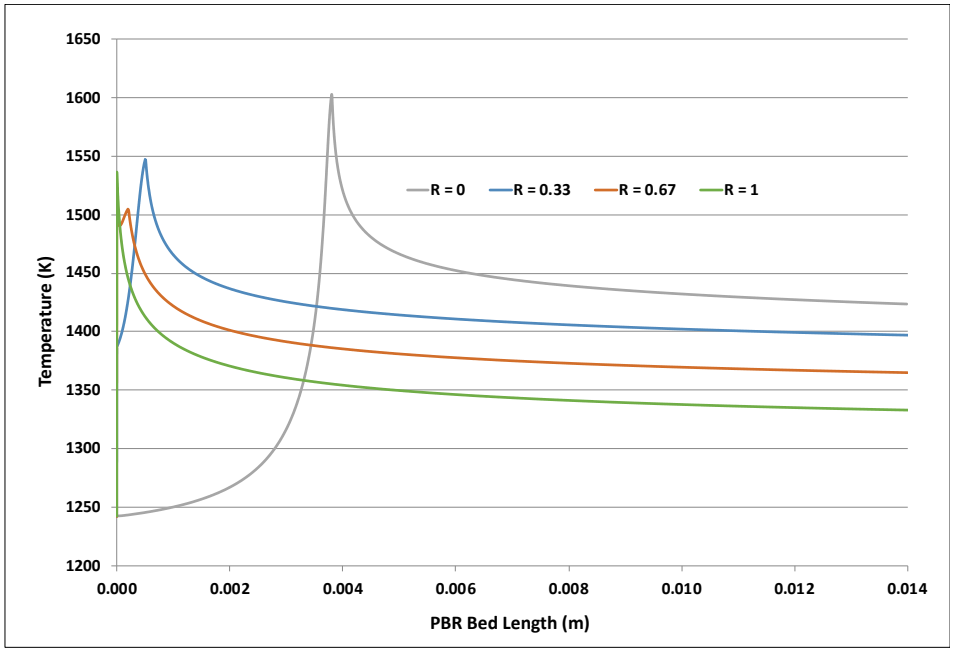

Figure 1. Impact of H_2O_2 content in feed oxidant; PBR LR_LF case at 1243 K feed; curves are different feed molar values $R \equiv H_2O_2/(O_2 + H_2O_2)$.

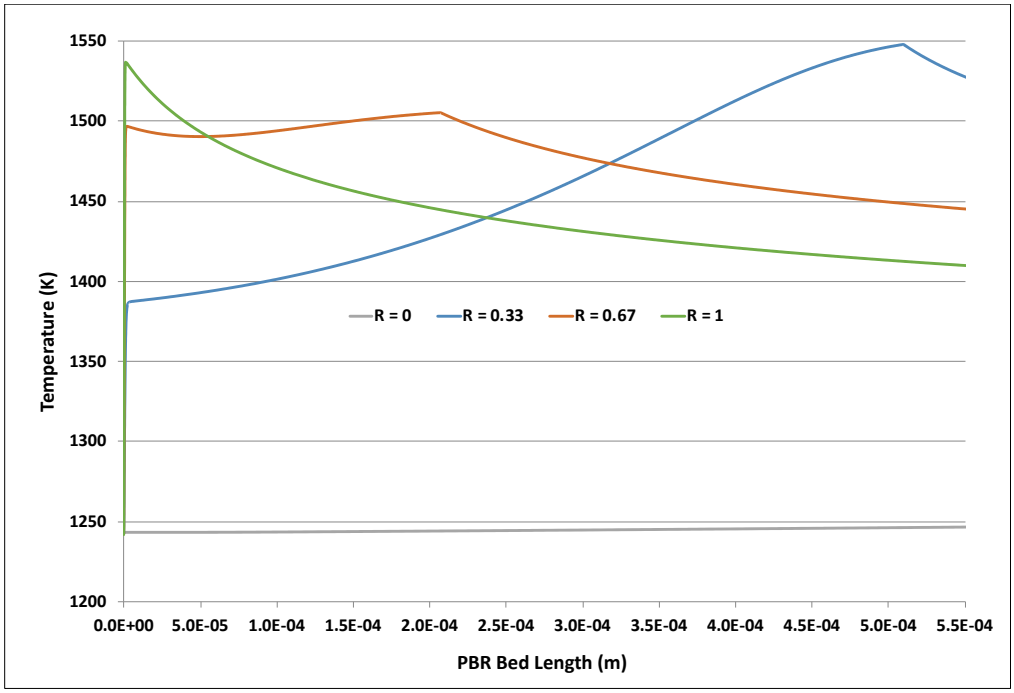

Figure 2. Post-entrance region of PBR for LR_LF case at 1243 K feed; curves are different feed molar values $R \equiv H_2O_2/(O_2 + H_2O_2)$.

Figure 3 shows that increasing the H_2O_2 content improved the selectivity of sum_C_2H_x, while lowering both the selectivity and yield for syngas (H_2 + CO). There was a negligible impact on sum_C_2H_x yields. The reduction in syngas was due almost entirely to a reduction in CO. Finally, for these four cases from R = 0 to 1, the CH_4 conversions were: 39.3, 36.6, 35.1, and 33.8%, respectively. In all cases, the final O_2 and H_2O_2 conversions were 100%.

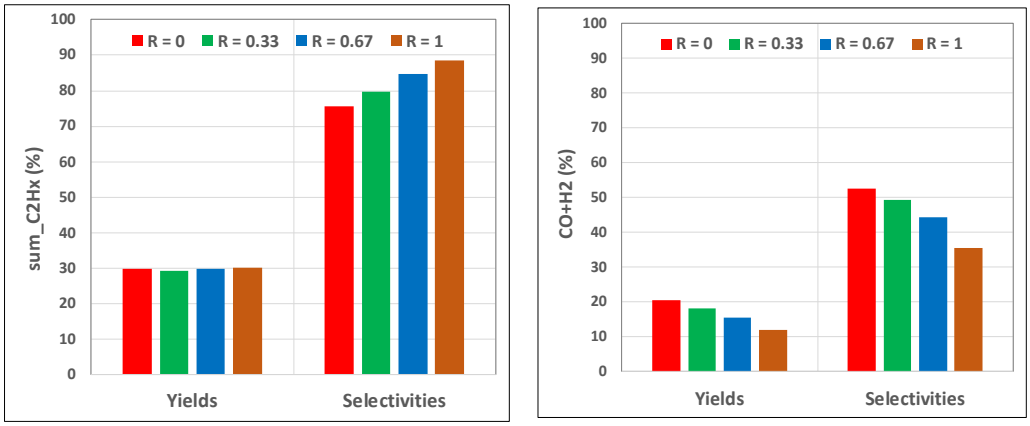

Figure 3. Impact of H_2O_2 content in feed oxidant; PBR LR_LF case at 1243 K feed; $R \equiv H_2O_2/(O_2 + H_2O_2)$. Values are based on PBR outlet; (**left**) $sumC_2H_x = C_2H_6 + C_2H_4 + C_2H_2$; (**right**) $CO + H_2$.

An expanded look at the long-post-entrance region provides more insight into the dramatic impact of substituting some of the feed O_2 with H_2O_2 vapor. Figure 4 shows the selectivities for the CO, C_2H_6, C_2H_4, and CH_4 conversions for the LR_LF case, at 1243 K feed temperature, for feed ratio cases R = 0 and R = 0.33. The curves were almost unchanged after the 0.006 m bed length was reached.

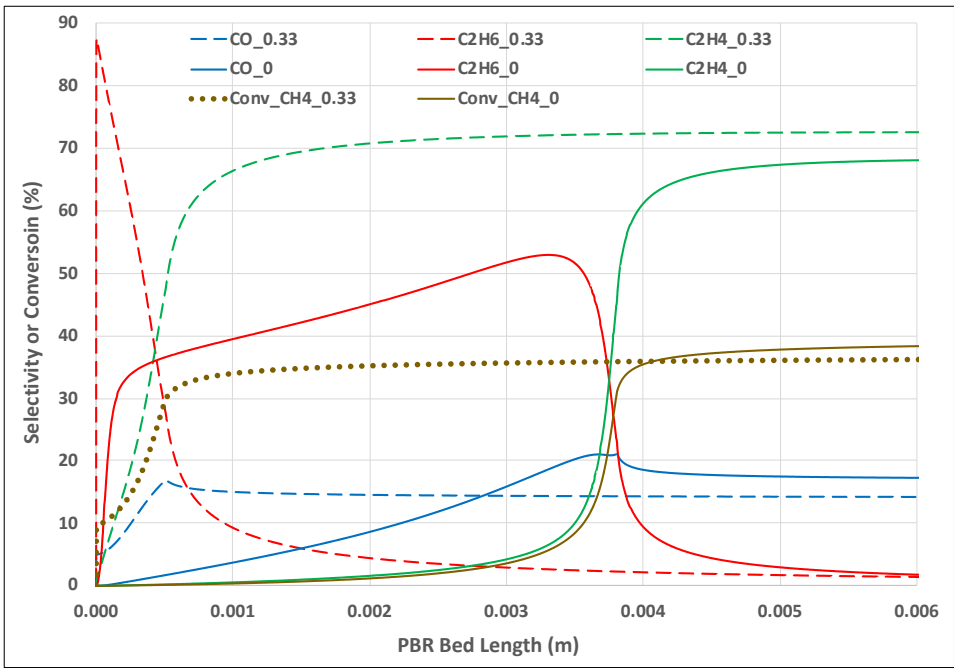

Figure 4. PBR long-post-entrance region for LR_LF case, 1243 K feed; key sensitivities and conversions for R = 0, 0.33 oxidant ratios.

Some key points can be made here. In the R = 0 case, CO selectivity exceeded C_2H_4 before the temperature peaked (see Figure 1), but was lower than C_2H_6. After the peak temperature, consistent with experimental observations by Liu et al. [12], C_2H_4 exceeded CO. In the R = 0.33 case, the H_2O_2 (not shown) dissociated immediately upon entry. The resulting •OH radicals abstracted •H atoms from CH_4, causing a spike in C_2H_6 formation, and a quickly rising CH_4 conversion. The C_2H_6 rapidly dehydrogenated to C_2H_4. The CO peaked at approximately where the temperature peaked. Unlike the R = 0 case, both C_2 species exceeded CO prior to the temperature peak. This all occurred much faster than

for the R = 0 case. The ultimate CH_4 conversion for the R = 0.33 case was only slightly lower than for the R = 0 case, while showing a higher C_2H_4 selectivity and lower CO. Liu et al. [12], for the R = 0 case, concluded that the selectivities of COx and C_2 depended on local O_2 concentration and temperature. Using H_2O_2 added the further complexity of gas phase chemistry to the surface reactions.

3.2. Use of H_2O_2 to Decrease Feed Temperature to PBR

We now discuss whether the replacement of O_2 by H_2O_2 allows for a lowering of the overall PBR feed temperature, which would be an energy and cost saving. This analysis used the R = 0 and R = 0.33 feeds with the LR_LF case, with the results shown in Table 2.

Table 2. Impact of partial replacement of feed O_2 by H_2O_2 at various feed temperatures for PBR running LR_LF case.

Feed Temperature (K)	1243	1143	1043	1043	943	943
R value	0	0	0	0.33	0	0.33
Max Temp (K)	1603	1547	1065	1414	944	1345
Exit Temp (K)	1424	1423	1065	1343	944	1321
CH_4 Conv (%)	39.3	33.8	0.891	26.4	0.044	21.8
sum_C_2H_x Selec (%)	75.6	72.3	58.7	70.0	36.7	62.6
sum_C_2H_x Yield (%)	29.7	24.4	0.522	18.5	0.016	13.6
CO + H_2 Sel. (%)	52.4	51.6	24.3	54.5	10.2	57.8
CO + H_2 Yield (%)	20.6	17.5	0.217	14.4	0.004	12.6

The partial H_2O_2 substitution for O_2 produced a respectable CH_4 conversion at the lower feed temperatures where O_2 feed alone showed no OCM activity (R = 0 for 1043 and 943 K feeds). These results at lower feed temperatures were consistent with those observed experimentally [17–19]. At the 843 K feed temperature, even the R = 0.33 case was poor.

3.3. Incremental H_2O_2 Replacing O_2 to CSTR

As mentioned above, the CH_4/O_2 and H_2O/H_2O_2 vapor streams would likely be fed separately into the CSTR due to safety concerns about preheating a vapor stream containing H_2O_2. For example, for the R = 0.33 and HR_HF case, to achieve an effective (hypothetical) 843 K feed temperature while holding the H_2O/H_2O_2 stream at 373 K, the CH_4/O_2 stream would be preheated to about 883 K. The HR_HF case was chosen for this CSTR analysis because it showed the best yield and selectivity of sum_C_2H_x at the lowest feed temperatures in the earlier study [11].

For the CSTR calculations, the volume was the same as the open (gas) volume of the packed bed, with the same catalyst surface area. The CSTR might be a single-phase ideal fluidized bed, or a perfectly mixed (e.g., jet-stirred) reactor with catalyst on the walls.

Substitution of all or some of the feed O_2 content with H_2O_2 had a marked impact on the CSTR performance. Figure 5 (left) shows that substituting H_2O_2 for O_2 reduced the exit temperature somewhat (~65–110 K), as might be expected from the lower exothermicity (see Equations (2) and (3)). However, Figure 5 (right) shows a complex story for the impact on CH_4 conversion. For effective feed temperatures of 843 and 943 K, switching from O_2 to H_2O_2 reduced CH_4 conversion by only ~3 percentage points. With a 1043 K feed temperature, there was little impact on conversion. At 1143 and 1243 K, switching to H_2O_2 actually increased CH_4 conversion. While literature experiments [17–19] used a PBR, the results here were still found to be consistent with those observations in terms of the activity of H_2O_2.

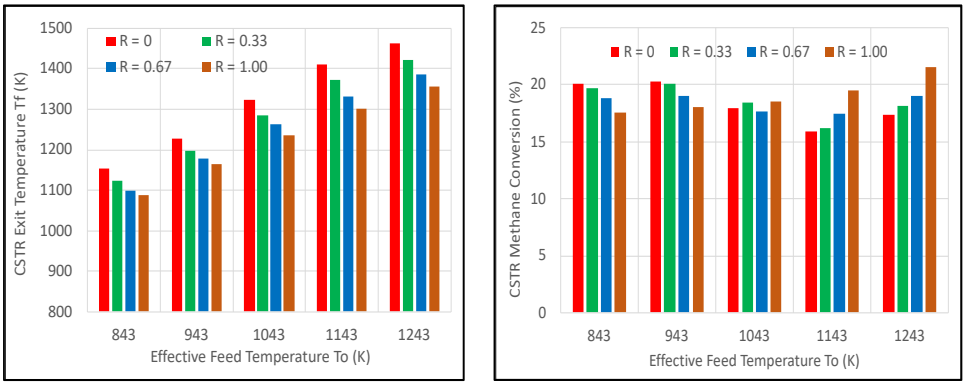

Figure 5. Impact of H_2O_2 content in feed oxidant on CSTR exit temperature (**left**) and CH_4 conversion (**right**) for HR_HF case where molar R = $H_2O_2/(O_2 + H_2O_2)$.

Figure 6 shows that the yield of sum_C_2H_x was notably higher than the CO + H_2 yield for all R cases, while increasing H_2O_2 had a greater impact on yields at the higher feed temperatures. These results were consistent with those revealed in Figure 3 for the PBR. Selectivities of sum_C_2H_x remained higher than CO + H_2, especially at the lower feed temperatures, as seen in Figure 7.

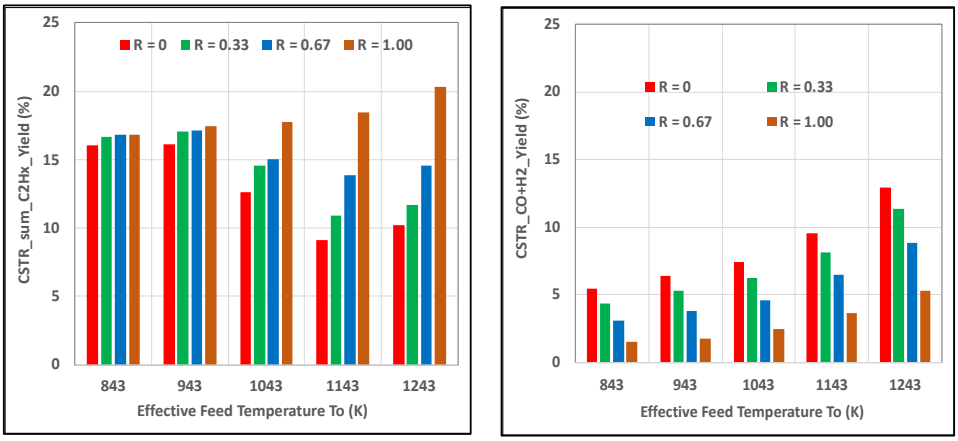

Figure 6. Impact of H_2O_2 content in feed oxidant on sum_C_2H_x and CO + H_2 yields in CSTR for HR_HF case where molar R = $H_2O_2/(O_2 + H_2O_2)$; (**left**) sumC_2H_x = C_2H_6 + C_2H_4 + C_2H_2; (**right**) CO + H_2.

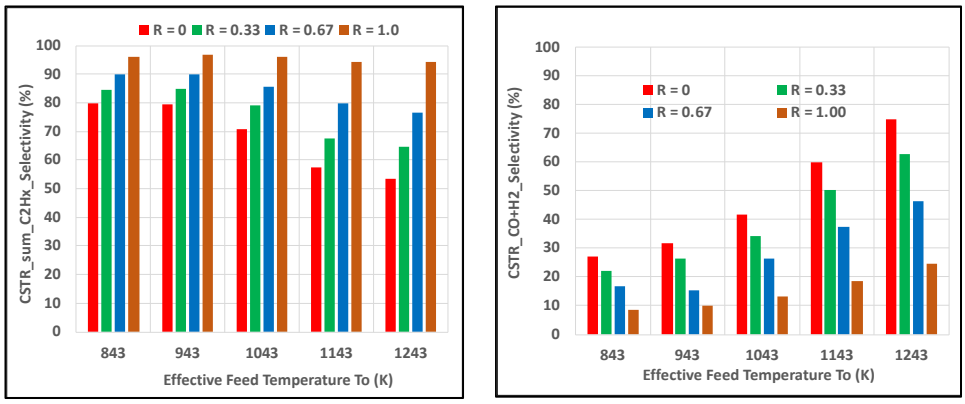

Figure 7. Impact of H_2O_2 content in feed oxidant on sum_C_2H_x and CO + H_2 selectivities in CSTR for HR_HF case where molar R = $H_2O_2/(O_2 + H_2O_2)$; (**left**) sumC_2H_x = C_2H_6 + C_2H_4 + C_2H_2; (**right**) CO + H_2.

Equations (2) and (3) suggest that replacing O_2 by H_2O_2 will increase the production of C_2H_4 and H_2O, while reducing CO and H_2. Consider the HR_HF case, with the effective feed temperature into the CSTR of 1243 K, with the results shown in Table 3. As the H_2O_2 fraction in the oxidant increased (i.e., higher R value), the CSTR exit temperature fell, but the CH_4 conversion increased. The C_2H_4 and H_2O production increased, while CO and H_2 dropped. Finally, the fraction of catalytic sites occupied by adsorbed O atoms (O_s) decreased as R increased. Since •H abstraction by •O_s is the primary catalytic step for CH_4 activation [6] by O_2, the drop in •O_s fraction was consistent with a shift from heterogeneous catalyzed to homogeneous non-catalyzed conversion pathways at higher R.

Table 3. Impact of progressive replacement of feed O_2 by H_2O_2 at 1243 K effective feed temperatures for CSTR running HR_HF case. * H_2O values are corrected for H_2O in feed for R $\neq$ 0 cases.

R Value	0	0.33	0.67	1
Exit Temp (K)	1463	1421	1386	1356
CH_4 Conv (%)	17.3	18.1	19.0	21.5
C_2H_4 Selec (%)	46.1	52.6	58.8	70.0
C_2H_4 Yield (%)	7.98	9.50	11.2	15.1
H_2O Selec (%) *	29.1	34.3	38.5	42.1
H_2O Yield (%) *	5.03	6.19	7.32	9.07
CO Selec (%)	35.1	26.7	14.9	0.10
CO Yield (%)	6.05	4.82	2.84	0.02
H_2 Selec (%)	39.8	36.1	31.5	24.5
H_2 Yield (%)	6.89	6.51	5.99	5.27
O_s coverage (ppm)	24.5	15.8	9.61	0.48

3.4. Brief Reactor Comparison Summary

A simple comparison between the PBR and CSTR for OCM with and without H_2O_2 as an activating oxidant is shown in Table 4. This illustration is based on the LR_LF case (see Table 1). The results will vary somewhat for other cases, but the observations will be similar. This summary considers both the current results and those published earlier with just O_2 as an activator [11]. While the claims are based on calculations using the Karakaya et al. [6] mechanism for La_2O_3/CeO_2 catalyst, it is anticipated other OCM catalysts would give rise to similar claims.

Table 4. Brief comparison of PBR vs. CSTR for OCM using the LR_LF case and R = 0.33 for the O_2/H_2O_2 runs.

	PFR	**PFR**	**CSTR**	**CSTR**
	O_2	**O_2/H_2O_2**	**O_2**	**O_2/H_2O_2**
Lowest practical feed temperature (K)	1143	943	843	843
CH_4 conversion	34	22	23	28
Sum_C_2Hx selectivity	72	63	55	80
CO + H_2 selectivity	52	58	57	33

Table 4 shows several points. The lowest practical feed temperature is the value below which there is no appreciable CH_4 conversion. All remaining values in each column correspond to those temperatures. Replacing a portion of the feed O_2 with H_2O_2 vapor allows the CSTR to achieve good CH_4 conversions at the lowest feed temperature. It also allows the PBR to run with a reduced feed temperature. Even at this low feed temperature, the CSTR has a sum_C_2H_x selectivity that exceeds the PBR at a much higher temperature. The CSTR also shows reduced syngas (CO + H_2) and improved sum_C_2H_x selectivity when using the H_2O_2.

4. Simple Layout of a "Green" OCM Plant

Although Equations (2) and (3) show that OCM via O_2 and H_2O_2 is exothermic, a future sustainable OCM plant must consider O_2 and H_2O_2 production and overall plant heat integration. Figure 8 offers a simple schematic. The OCM reactor feeds CH_4 and a combination of O_2 and vapor phase moist H_2O_2. The O_2 is produced in a solar powered air separation plant [23] that enjoys the energy and economic savings from chemical looping instead of cryogenic separation [24,25]. Aqueous H_2O_2 is produced by the solar powered catalyzed reaction of O_2 and acidic liquid H_2O [20]. Vapor phase H_2O_2 is stripped out of the liquid by the N_2 or He [21] recovered from the natural gas. Heavier-than-CH_4 saturated hydrocarbons (C_2H_6-C_5H_{12}) are separated out from the natural gas. Post-OCM reactor processing separates the CO and H_2 as synthesis gas and the desirable coupled hydrocarbons (e.g., C_2H_4 and C_2H_6). Byproduct CO_2 from Separations_2 and Pretreatment can be captured with caustic scrubbing, and subsequently sequestered.

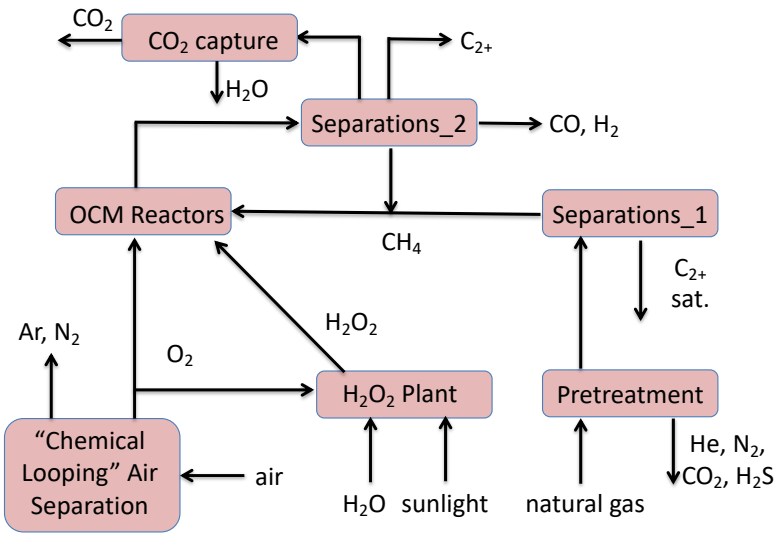

Figure 8. Hypothetical "green" OCM plant utilizing solar-powered H_2O_2 production and chemical looping for air separation.

5. Conclusions

Using an elementary reaction mechanism for the oxidative coupling of methane (OCM) on a La_2O_3/CeO_2 catalyst borrowed from the literature, this study considered the incremental replacement of the activating O_2 with moist H_2O_2 vapor. Both packed bed reactor (PBR) and continuous stirred tank reactor (CSTR) configurations were used. As the H_2O_2 content of the oxidant increased, more of the CH_4 conversion occurred in the gas phase with less assistance from the catalytic surface. Hydroxyl (•OH) radicals from rapid H_2O_2 decomposition abstracted •H atoms from CH_4 to produce •CH_3 radicals. This occurred in parallel to a similar abstraction by oxygen atoms (•O_s) adsorbed on the catalyst surface when O_2 was fed. In the PBR, H_2O_2 allowed the "light-off" temperature jump to occur using a lower feed temperature. Even though there was a slight decline in CH_4 conversion, the C_2H_x selectivity increased while synthesis gas dropped. Since significant preheat was still needed, process safety considerations might dictate that H_2O_2 vapor is better suited to the continuous stirred tank reactor (CSTR) configuration where the H_2O_2/H_2O vapor stream can be fed at lower temperatures separately from the preheated CH_4/O_2 stream. In a CSTR, H_2O_2 significantly improved C_2H_x production compared to synthesis gas over all feed temperatures studied, thus showing that OCM is possible with significantly less preheating compared to PBR. A future OCM plant can operate in a more "green" way with the use of solar-activated H_2O_2 production, and solar-powered O_2 production from chemical-looping air separation.

Author Contributions: A.M.—calculations, S.R.—calculations, P.P.—calculations, M.L.—calculations, R.B.—calculations, writing, supervision, total responsibility. All authors have read and agreed to the published version of the manuscript.

Funding: This research received no external funding.

Institutional Review Board Statement: Not applicable.

Informed Consent Statement: Not applicable.

Data Availability Statement: Supporting data are not posted, but are available upon request.

Acknowledgments: The authors appreciate the support of Canan Karakaya in using Detchem®.

Conflicts of Interest: The authors declare no conflict of interest.

Sample Availability: Compound samples are not available from the authors.

References

1. Yang, S.; Dezember, R. The U.S. Is Overflowing with Natural Gas. Not Everyone Can Get It. *Wall Street J.* 8 July 2019. Available online: https://www.wsj.com/articles/the-u-s-is-overflowing-with-natural-gas-not-everyone-can-get-it-11562518355 (accessed on 8 July 2019).
2. Kohler, J. Colorado Regulators Give Initial OK to Ban on Flaring of Oil, Gas Wells to Curb Methane Pollution. *The Denver Post*. Available online: https://www.denverpost.com/2020/11/06/colorado-venting-flaring-oil-gas-wells-methane-pollution (accessed on 6 November 2020).
3. NMOGA. New Mexico Oil & Gas Association. Available online: https://www.nmoga.org/exxon_mobil_to_use_satellites_to_detect_methane_emissions_in_permian_basin (accessed on 17 December 2021).
4. Karakaya, C.; Morejudo, S.H.; Zhu, H.; Kee, R.J. Catalytic chemistry for methane dehydroaromatization (MDA) on a bifunctional Mo/HZM-5 catalyst in a packed bed. *Ind. Eng. Chem. Res.* **2016**, *55*, 9895–9906. [CrossRef]
5. Stansch, Z.; Mleczko, L.; Baerns, M. Comprehensive Kinetics of Oxidative Coupling of Methane over the La_2O_3/CaO Catalyst. *Ind. Eng. Chem. Res.* **1997**, *36*, 2568–2579. [CrossRef]
6. Karakaya, C.; Zhu, H.; Zohour, B.; Senkan, S.; Kee, R.J. Detailed Reaction Mechanisms for the Oxidative Coupling of Methane over La2O3/CeO2 Nanofiber Fabric Catalysts. *Chem. Cat. Chem.* **2017**, *9*, 4538–4551.
7. Gambo, Y.; Jalil, A.A.; Triwahyono, S.; Abdulrasheed, A.A. Recent Advances and future prospect in catalysts for oxidative coupling of methane to ethylene: A review. *J. Ind. Eng. Chem.* **2018**, *59*, 218–229. [CrossRef]
8. Siluria. 2014. Available online: http://siluria.com/Technology/Demonstration_Plant (accessed on 11 January 2022).
9. Department of Energy (DOE). 2017. Available online: https://www.osti.gov/servlets/purl/1414280 (accessed on 11 January 2022).
10. Cruellas, A.; Melchiori, T.; Gallucci, F.; van Sint Annaland, M. Advanced reactor concepts for oxidative coupling of methane. *Cat. Rev.* **2017**, *59*, 234–294. [CrossRef]
11. Rivera, S.; Molla, A.; Pera, P.; Landaverde, M.; Barat, R. Reactor engineering calculations with a detailed reaction mechanism for the oxidative coupling of methane. *Int. J. Chem. React. Eng.* **2020**, *18*. [CrossRef]
12. Liu, Z.; Li, J.P.H.; Vovk, E.; Zhu, Y.; Li, S.; Wang, S.; van Bavel, A.P.; Yang, Y. Online Kinetics Study of Oxidative Coupling of Methane over La_2O_3 for Methane Activation; What is Behind the Distinguished Light-Off Temperatures? *ACS Catal.* **2018**, *8*, 11761–11772. [CrossRef]
13. Beck, B.; Fleischer, V.; Arndt, S.; Hevia, M.; Urakawa, A.; Hugo, P.; Schomacker, R. Oxidative coupling of methane—A complex surface/gas phase mechanism with strong impact on the reaction engineering. *Cat. Today* **2014**, *228*, 212–218. [CrossRef]
14. Chen, Q.; Couwenberg, P.M.; Marin, G.B. Effect of pressure on the oxidative coupling of methane in the absence of catalyst. *AIChE J.* **1994**, *40*, 521–535. [CrossRef]
15. Alexiadis, V.; Thybaut, J.; Kechagiopoulos, P.; Chaar, M.; Van Veen, A.; Muhler, M.; Marin, G. Oxidative coupling of methane: Catalytic behavior assessment via comprehensive microkinetic modeling. *Appl. Cat. B Environ.* **2014**, *150–151*, 496–505. [CrossRef]
16. Deutschmann, O.; Tischer, S.; Correa, C.; Chatterjee, D.; Kleditzsch, S.; Janardhanan, V.M.; Mladenov, N.; Minh, H.D.; Karadeniz, H.; Hettel, M. *DETCHEM Software Package, 2.5 ed.*; DETCHEM: Karlsruhe, Germany, 2014; Available online: www.detchem.com (accessed on 11 January 2022).
17. Garibyan, T.; Muradyan, A.; Grigoryan, R.; Vartikyan, L.; Minasyan, V.; Manukyan, N. New methods of increasing the catalytic activity and selectivity in the oxidative conversion processes of methane and propylene. *Cat. Today* **1995**, *24*, 249–250. [CrossRef]
18. Eskendirov, I.; Coville, N.J.; Sokolovskii, V. Methane oxidative coupling on the Au/La_2O_3/CaO catalyst in the presence of hydrogen peroxide. *Cat. Lett.* **1995**, *35*, 33–37. [CrossRef]
19. Eskendirov, I.; Coville, N.; Parmaliana, A.; Sokolovskii, V. Direct oxidative conversion of methane into higher hydrocarbons and oxy-products in the presence of hydrogen peroxide. In *Natural Gas Conversion IV*; de Pontes, M., Espinoza, R., Nicolaides, C., Scholz, J., Scurrell, M., Eds.; Studies in Surface Science and Catalysis; Elsevier: Amsterdam, The Netherlands, 1997; Volume 107, pp. 301–306.

20. Kaynan, N.; Berke, B.A.; Hazut, O.; Yerushalmi, R. Sustainable photocatalytic production of hydrogen peroxide from water and molecular oxygen. *J. Mat. Chem. A.* **2014**, *2*, 13822–13826. [CrossRef]
21. Spiegelman, J.; Alvarez, D. Cheating Raoult's Law to Enable Delivery of Hydrogen Peroxide as a Stable Vapor. Available online: https://www.peroxidizer.com/resources/articles/article-Cheating-Raoults-Law-Stabilized-Hydrogen-Peroxide-Vapor.pdf (accessed on 11 January 2022).
22. Satterfield, C.; Stein, T. Decomposition of Hydrogen Peroxide Vapor on Relatively Inert Surfaces. *Ind. Eng. Chem.* **1957**, *49*, 1173–1180. [CrossRef]
23. Patzschke, C.F.; Bahzad, H.; Boot-Handford, M.E.; Fennell, P.S. Simulation of a 100-MW solar-powered thermo-chemical air separation system combined with an oxy-fuel power plant for bio-energy with carbon capture and storage (BECCS). *Mitig. Adapt. Strateg. Glob. Change* **2020**, *25*, 539–557. [CrossRef]
24. Qing, M.; Jin, B.; Ma, J.; Zou, X.; Wang, X.; Zheng, C.; Zhao, H. Thermodynamic and economic performance of oxy-combustion power plants integrating chemical looping air separation. *Energy* **2020**, *206*, 118136. [CrossRef]
25. Shah, K.; Moghtaderi, B.; Wall, T. Chemical Looping Air Separation (CLAS) for Oxygen production: Thermodynamic and Economic Aspects. In Proceedings of the Australian Combustion Symposium, Newcastle, Australia, 29 November–1 December 2011; pp. 240–243.